Eur. J. Mineral., 35, 373–382, 2023
https://doi.org/10.5194/ejm-35-373-2023

European Journal of Mineralogy
Open Access

Fe-bearing vanadium dioxide–paramontroseite: structural details and high-temperature transformation

Nadia Curetti and Alessandro Pavese

Earth Sciences Department, University of Turin, Via Valperga Caluso 35, 10125 Turin, Italy

Correspondence: Nadia Curetti (nadia.curetti@unito.it)

Received: 20 November 2022 – Revised: 5 April 2023 – Accepted: 2 May 2023 – Published: 1 June 2023

Abstract. A natural sample of Fe-bearing paramontroseite ($V_{0.84}Fe_{0.19}Al_{0.03}O_2$; $a = 4.8960(14)$, $b = 9.395(3)$, $c = 2.9163(5)$ Å, $V = 134.14(6)$ Å^3; space group *Pbnm*) from Prachovice mine (Czech Republic) was investigated to shed light on cation partitioning and behavior upon heating. XRD experiments showed that V and Fe are not vicariant of one another, as V occupies the octahedral site at (0.09, 0.14, 0.25), whereas Fe enters a tetrahedral site at (0.41, 0.06, 0.25), the latter expected to be empty in the ideal structure. Thermal expansion is anisotropic, leading to the following β coefficients: -2.0×10^{-5}, 3.0×10^{-5}, 0.8×10^{-5} and 1.8×10^{-5} °C^{-1} for a, b, c and V, respectively. At T higher than 350 °C, V undergoes oxidation, from [4+] to [5+], and paramontroseite decomposes into Fe-tetrapolyvanadate ($Fe_2V_4O_{13}$) and V-pentoxide (V_2O_5). μ-Raman spectroscopy analyses confirmed that paramontroseite is sensitive to heating: the crystal surface invested by the laser beam degrades very quickly, leading to the phases revealed by diffraction measurements. There is no evidence for the formation at high T of a rutile-type phase, as we observed for iso-structural ramsdellite MnO_2.

1 Introduction

Vanadium is a multivalent transition metal, forming a large number of different oxides: VO, VO_2 (at least 14 different crystal structures are known for VO_2), V_2O_3, V_2O_5, V_3O_5, V_3O_7 and more; a complete review of the synthetic V compounds is reported in the work of Shvets et al. (2019).

Interest in V has recently grown in relation to the increasing sensitivity to environmentally sustainable energy solutions. In fact, vanadium has chemical–physical features making it suitable for use in many technological applications including catalysis (Wachs, 2013), batteries (Mingzhe et al., 2020), electrochromic systems and solar windows (Fortier et al., 2014), and supercapacitors (Ndiaye et al., 2019). Accurate characterizations of the vanadium oxide phases, both synthetic and natural, can be helpful in improving general knowledge about these materials and optimizing their potential uses.

In nature, the most common mineralogical "V phases" (i.e., phases in which V is the only cation, whereas anions can be provided by O and OH groups) are montroseite VO(OH) and paramontroseite VO_2, where V has oxidation states [+3] and [+4], respectively.

Montroseite was first identified in the mid-20th century in Colorado (Weeks et al., 1953; Evans and Block, 1953), during the study and related characterization of a vanadium–uranium mine. The name comes from Montrose County, the locality where it was first found (Bitter Creek Mine). Montroseite, space group *Pbnm* ($a = 4.54$ Å, $b = 9.97$ Å, $c = 3.03$ Å), occurs in black, opaque, submetallic and bladed crystals and belongs to the same mineral group of diaspore AlO(OH), goethite FeO(OH) and groutite MnO(OH). The building unit of the structure is the V-centered octahedron, wherein the vanadium atom is surrounded by four equatorial oxygens (O_{eq}) and two axial oxygens (O_{ax}). Each V octahedron shares three edges with as many building units, and pairs of octahedral chains develop parallel to z. Double chains are interconnected by sharing corners and originate channels, parallel to z. These channels have rectangular cross sections, equal in size to two side-by-side octahedra; inside the channels, H atoms are arranged, bonded to oxygens.

Evans and Mrose (1955) carried out studies of montroseite from Bitter Creek Mine and found that it is associated with another V phase, i.e., *paramontroseite*. The unit cell volume of the latter is slightly smaller ($a = 4.89$, $b = 9.39$,

$c = 2.93$ Å), and the structure corresponds to ramsdellite's (see below, Fig. 4a). The cited authors assumed that paramontroseite is a natural weathering product from montroseite, according to the reaction below:

$$2\,\mathrm{VO(OH)} + \frac{1}{2}\mathrm{O_2} \rightarrow 2\,\mathrm{VO_2} + \mathrm{H_2O},$$

where vanadium is oxidized from [+3] to [+4], through a reduction of available oxygen and consequent loss of hydrogen.

Natural samples of both montroseite and paramontroseite usually contain a significant amount of Fe. Weeks et al. (1953) report an FeO content of ∼ 8.8 wt % in paramontroseite samples from Colorado; no analysis of the oxidation state of iron is mentioned, and the authors suggest that Fe^{2+} occurs on account of the cation replacement with V^{4+} in octahedral coordination. Another relevant vanadium–uranium mineralization was found in the large active quarry of Prachovice (eastern Bohemia, Czech Republic); paramontroseite from this site contains 21.5 wt %–28.1 wt % of Fe_2O_3 (Sejkora et al., 2013). Structural adjustments to accommodate Fe^{3+} have not been investigated so far.

In view of the structure analogy between paramontroseite and ramsdellite (MnO_2) and of the phase transition to which the latter is subject at ∼ 310 °C (amorphization and re-crystallization into pyrolusite; Curetti et al., 2021), we expect that paramontroseite also undergoes a transformation as a function of temperature. To our knowledge, paramontroseite at high temperature has never been investigated hitherto. All this has motivated the present study, which aims to fill such a gap by providing a description of the stability and structural behavior of paramontroseite upon heating up to 550 °C.

2 Materials and experimental methods

2.1 Sample

The sample under investigation is a natural paramontroseite from the vanadium–uranium mineralization of Prachovice, in the Czech Republic. In our specimen, the crystals, which are strewn over a carbonate matrix ($3 \times 4\,\mathrm{cm^2}$), show an opaque black color and regular lamellar shape (Fig. 1), with a maximum elongation of ∼ 7–8 mm and development normal to the matrix. Among the lamellae of paramontroseite, one can distinguish calcite and small crystals of a transparent yellow-greenish color, identified by chemical analyses as a uraninite-like phase.

2.2 Chemical maps and analyses

Sample fragments ($\sim 5 \times 5 \times 3\,\mathrm{mm^3}$ in size) of the specimen in Fig. 1 were polished, carbon coated and analyzed using a JEOL JSM-IT300LV Scanning Electron Microprobe, equipped with an Oxford INCA Energy 200 EDS SATW detector (working distance 10 mm, 15 kV).

Composition maps were recorded to investigate the distribution of the main chemical elements in the original sample. In Fig. 2 we can recognize paramontroseite, calcite and a uraninite-like phase; small Pb-rich areas are associated with uraninite. In some cases, the uraninite crystals are arranged so as to rim in earlier-formed paramontroseite, on which heterogeneous nucleation and growth of the former probably took place.

Quantitative chemical analyses were performed on the paramontroseite crystals, using as standards almandine (Al), magnetite (Fe), vanadium (V) and uraninite (U). We estimate an uncertainty of ∼ 0.01 atoms per formula unit (a.p.f.u.), based on instrument calibration and detection limit. An attentive inspection of well-developed and idiomorphic crystals reveals a core-to-rim zonation (Fig. 3). In the core the composition is provided by V only, whereas Fe and Al increase approaching the rim. The composition spans the following intervals: 96.3 wt %–74.6 wt %, 2.9 wt %–23.2 wt % and 0.8 wt %–2.3 wt % for VO_2, Fe_2O_3 and Al_2O_3, respectively. The resulting average formula unit calculated on the base of two oxygens is

$$\mathrm{V_{0.84}\,Fe_{0.19}\,Al_{0.03}\,O_2}.$$

The sum of the cations is slightly higher than 1 ($\sum = 1.06$), as reported and discussed by Sejkora et al. (2013). Paramontroseite crystals were picked up from the specimen and treated under high-temperature conditions (6 h heating at 400 °C). Such a thermal treatment did not induce any chemical zoning due to a possible intra-crystal Fe and V diffusion, as proven by EDS analyses.

2.3 Single-crystal X-ray diffraction

Single-crystal X-ray diffraction measurements were performed with a Gemini R Ultra Oxford diffractometer, equipped with an AtlasS2 CCD detector, using Mo$K\alpha$ radiation (generator operating at 50 kV/40 mA). Diffraction intensities were recorded from two crystals up to a 2θ angle of 70°, with a width angle of 1°. The 171-39-46 version of the CrysAlisPro software (Rigaku – Oxford Technologies) was used to integrate the reflection intensities and to account for absorption and Lorentz–polarization corrections. Structure refinement was carried out by the SHELX-97 package (Sheldrick, 2008), using the space group *Pbnm* and starting from the fractionary coordinates reported by Evans and Mrose (1955). The CSD-CCDC codes 2212426–2212427 contain the results from structure refinement and the calculated structure factors F_{hkl} (CIF and FCF files, both obtainable free of charge at https://www.ccdc.cam.ac.uk/structures, last access: 26 May 2023). Given that the two investigated crystals gave very similar results, we focus here on one sample only for brevity.

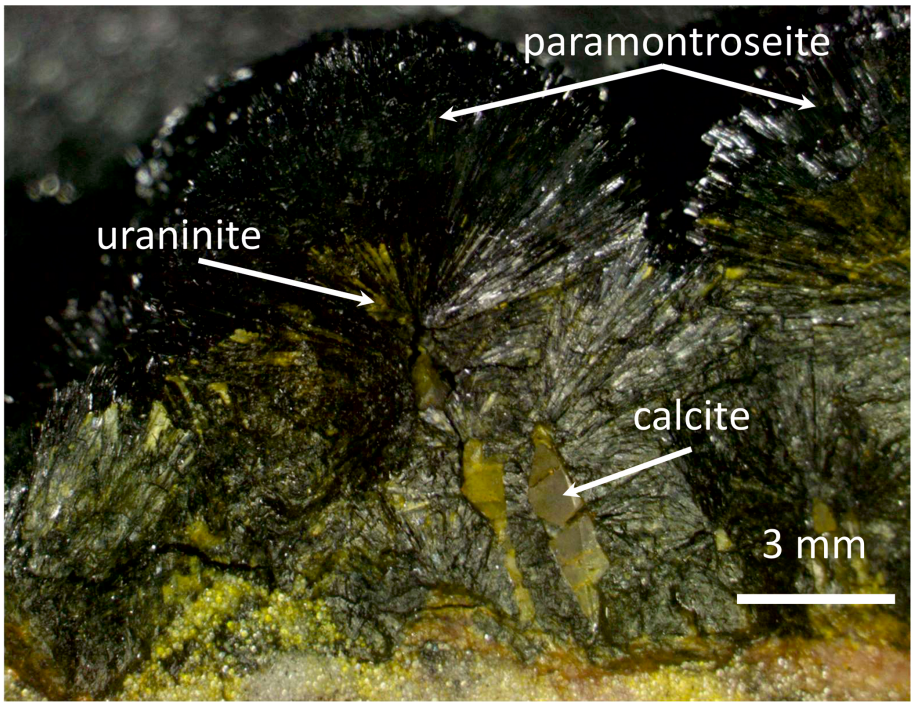

Figure 1. Main phases forming the original sample: paramontroseite (black idiomorphic lamellae), calcite (gray and interstitial) and uraninite-like phase (small and equidimensional yellow-greenish crystals).

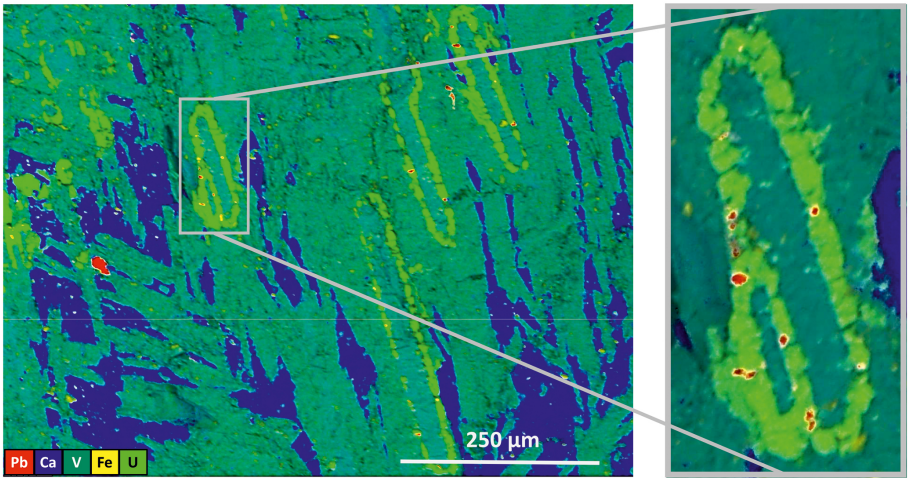

Figure 2. Composition map of the sample; areas rich in V (dark green – paramontroseite), Ca (blue – calcite), U (greenish-yellow) and Pb (red) are clearly distinct.

Preliminary results on untreated crystals show that the octahedral site (M) is not completely occupied (Table 1) and a residual electron density can be observed at a supposed empty tetrahedral site (T), lying within the [001] channels (Fig. 4b). We tested different cation distributions over M and T and concluded that the one having Fe^{3+} in T and V^{4+} in M is the closest to the experimental evidence. The measurement conditions and structural details are reported in Table 1.

2.4 In situ high-temperature X-ray powder diffraction

Paramontroseite crystals were selected and picked up from U-free areas of the rocky sample shown in Figs. 1 and 2 to carry out in situ high-temperature XRPD experiments. The sample so obtained still exhibited about 8 wt % calcite. The powder was placed in a flat Pt sample-holder and then in a high-temperature cell (multipurpose system – Rigaku). The actual temperature at the sample was determined through a

Table 1. Single-crystal X-ray diffraction measurement conditions and details from structure refinement of untreated paramontroseite. "GooF" denotes goodness of fit, and "sof" denotes site occupancy factor.

Measurement conditions		Bond distances (Å)		Bond angles (°)	
a	4.8960(14) Å	T–O1	1.825(4)	O2–T–O2	112.33(13)
b	9.395(3) Å	T–O2 (×2)	1.916(4)	O2–T–O2	112.5(2)
c	2.9163(5) Å	T–O2	1.754(2)	O2–T–O1	103.20(14)
V	134.14(6) Å^3	⟨T–O⟩	1.812(2)	O1–T–O2	112.63(18)
Space group.	*Pbnm*	M–O1	1.842(3)	O1–M–O1	96.25(5)
Cell refl.	515	M–O1 (×2)	1.984(2)	O1–M–O1	94.61(14)
Total refl.	6441	M–O2 (×2)	2.0098(18)	O1–M–O2	93.39(11)
Unique refl.	620	M–O2	2.143(3)	O1–M–O2	85.37(9)
$R_{\mathrm{Fo}>4\sigma(\mathrm{Fo})}$	6.08%	⟨M–O⟩	1.9954(16)	O1–M–O2	89.99(10)
wR^2	12.92%			O2–M–O2	93.02(11)
GooF	0.969			O2–M–O2	80.31(11)
				O1–M–O2	170.77(11)
	x	y	z	sof	U_{eq}
M	0.08872(19)	0.14280(11)	0.25	0.762(3) V	0.0215(2)
T	0.4075(5)	0.0595(3)	0.25	0.196(2) Fe	0.0116(6)
O1	0.1011(6)	−0.2463(3)	0.25	1.0 O	0.0241(7)
O2	−0.2278(6)	−0.0147(2)	0.25	1.0 O	0.0237(7)

calibration curve that relies upon solid–solid phase transitions (quartz and Na_2SO_4) and dilatation of standard materials (metallic Si and Pt), up to about 1000 °C. High-temperature in situ measurements were performed using a SmartLab XE powder diffractometer (Rigaku), with Cu$K\alpha$ radiation and an X-ray tube operating at 40 kV and 30 mA. XRPD patterns were recorded every 50 °C up to 550 °C. The sample was heated at a rate of 20 °C min^{-1}; once a given temperature had been reached, the related data collection started 2 h later for the system to achieve equilibrium. We used a 256-channel multi-strip detector moving with a speed of 0.6° min^{-1}, in the interval $10° < 2\vartheta < 90°$ at steps of 0.02° (about 150 min for each data collection period). We employed the GSAS-II software package (Toby and Von Dreele, 2013) for full profile fitting, adopting pseudo-Voigt profile functions to model the experimental patterns. Instrumental contributions to the peak shape, such as asymmetry and intrinsic peak broadening, were determined by means of a standard sample (LaB_6). We chose a refinement strategy based on varying (i) the profile function parameters associated with grain size and strain and (ii) the coefficients of the Chebyshev polynomial linear combination that models the background (Fig. 5). The relative intensity of the peaks did not suggest occurrence of preferred orientation of the crystallites in the sample. We did not refine structure parameters, using those at room temperature from the present work (paramontroseite) and from the literature ($V_4Fe_20_{13}$: Permer and Laligant, 1997; V_2O_5: Shklover et al., 1996). The small amount of calcite (stable in the T range investigated) was used as an internal check for the consistency of the results.

2.5 Raman spectroscopy on single crystals

Raman spectra were collected on both natural single crystals and HT-treated samples (6 h at 400 °C), using a LabRAM HRVIS – Horiba Jobin Yvon HR800 μ-Raman spectrometer (Giovanni Scansetti Interdepartmental Centre, University of Turin) equipped with a cooled CCD detector (−70 °C), Nd solid-state green laser (wavelength 532 nm, power 250 mW) and 600 grooves mm^{-1} grating, in the 60–1050 cm^{-1} range. Raman spectra were acquired with LabSpec 5 (Horiba) and treated with Fityk 0.9.8 software (Wojdyr, 2010) to compare such data with those from the RRUFF™ Project database (Lafuente et al., 2015).

3 Results and discussion

3.1 Single-crystal X-ray diffraction

The occurrence of Fe in natural montroseite and paramontroseite has long been known, but the present investigation provides new information on the cation arrangement in the oxygen framework. The refinement of the residual electronic density shows that V and Fe do not replace each other, but they occupy two different structure sites, M [0.0887(2), 0.1428(1), 0.25] and T [0.4075(5), 0.0595(3), 0.25], respectively. In M, the V–O bond distances (Table 1) are comparable to those reported for the paramontroseite from Colorado, ranging from 1.88 to 2.12 Å (Evans and Mrose, 1955). The four M–O_{eq} bond distances of the octahedral M site are close to each other [1.984(2) and 2.0098(18) Å], while the M–

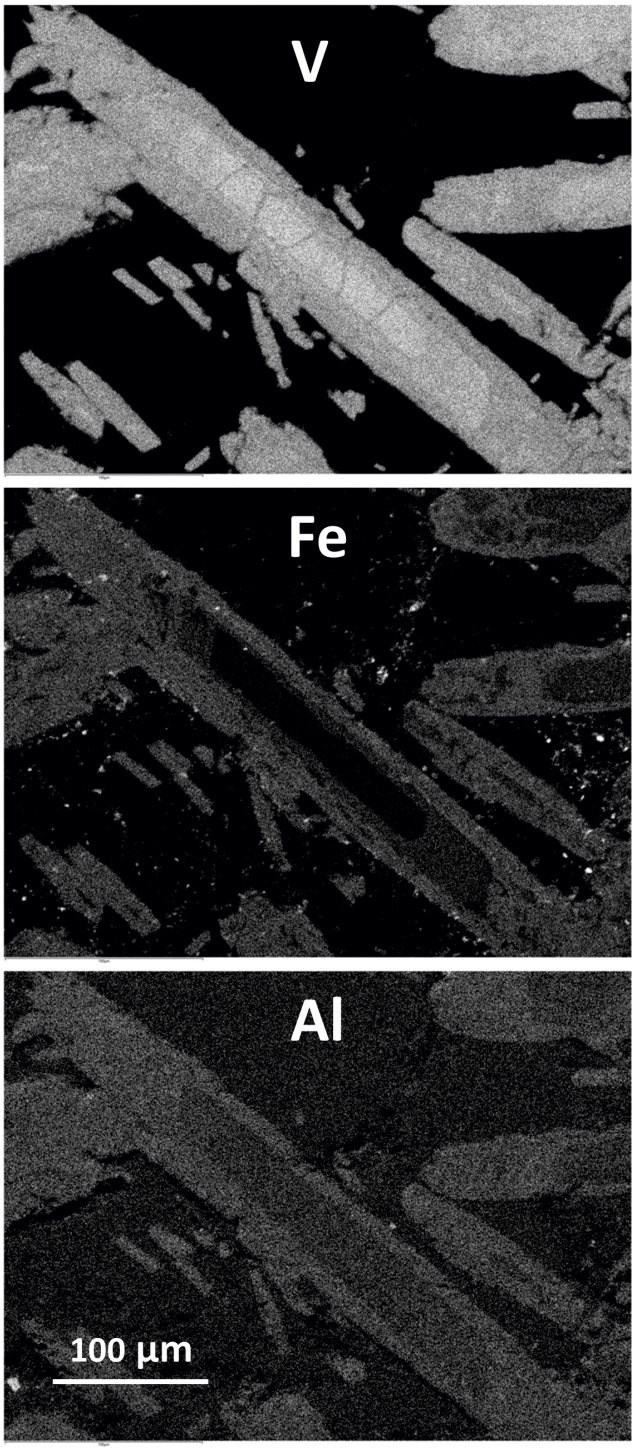

Figure 3. Core-to-rim zoning in an untreated single crystal of paramontroseite.

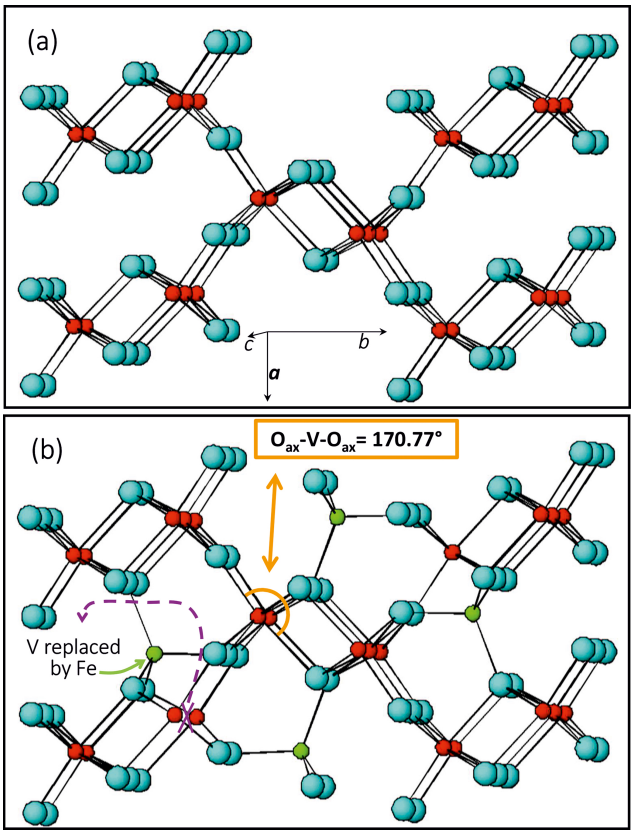

Figure 4. Comparison between structural details of V-pure **(a)** and Fe-bearing **(b)** paramontroseite; atom color: V, red; Fe, green; and O, light blue. Fe does not replace V but enters a different site, empty in the ideal structure.

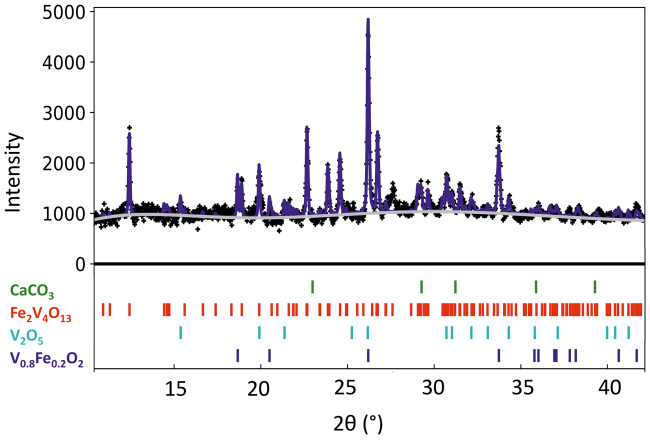

Figure 5. XRPD pattern recorded at 450 °C. The peaks of all the phases involved in the transformation are appreciable. The background was subtracted; figures of merit: wR = 3.76 %, GooF = 1.90.

Table 2. Proposed model for cation distribution in paramontroseite, over the M and T sites.

Site	Site content by stoichiometry	Electrons by chemical formula	Electrons by structure refinement
M	0.84 a_V.p.f.u.	19.32 e^-	17.53 e^-
T	0.19 a_{Fe}.p.f.u.	4.94 e^-	5.09 e^-

Table 3. Unit cell parameters for paramontroseite at high temperature.

T (°C)	a (Å)	b (Å)	c (Å)	V (Å^3)
25	4.896(9)	9.395(3)	2.9163(5)	134.14(6)
50	4.8956(3)	9.3978(5)	2.9172(2)	134.213(11)
100	4.9000(3)	9.4026(5)	2.9195(3)	134.512(13)
150	4.9065(4)	9.4166(7)	2.9155(4)	134.703(18)
200	4.9016(6)	9.4284(9)	2.9132(4)	134.629(19)
250	4.8920(5)	9.4408(8)	2.9139(3)	134.577(15)
300	4.8787(4)	9.4662(6)	2.91643(16)	134.689(10)
350	4.8714(4)	9.4864(6)	2.9196(16)	134.921(10)
400*	4.8684(2)	9.4967(8)	2.9241(3)	135.193(14)
450*	4.8582(5)	9.5038(9)	2.9308(3)	135.321(19)

* At $T > 350$ °C, paramontroseite becomes meta-stable.

O_{ax}'s are significantly either longer [2.143(3) Å] or shorter [1.842(3) Å] than ⟨M–O_{eq}⟩. This difference between the M–O_{ax} distances is associated with a different role played by the oxygen atoms involved in the framework: one O_{ax} is shared between two chains of the same pair (long distance), while the other O_{ax} is shared by chains of two distinct pairs (short distance) (Fig. 4).

The M–O_{ax}, i.e., V–O_{ax}, bond is normal to the plain of the four equatorial oxygen atoms, i.e., O_{eq}, in tetragonal symmetry (rutile-type structure), whereas the O_{ax}–M–O_{eq} angle is different from 90° in orthorhombic symmetry (axial bond squareness angle; Curetti et al., 2019). In ramsdellite and paramontroseite, the octahedra forming a pair of chains "tilt" towards each other, thus giving O_{ax}–M–O_{ax} angles that are smaller than 180° (Fig. 4b) and similar to each other, i.e., 170.45(14) and 170.77(11)°.

The average ⟨T–O⟩, i.e., ⟨Fe–O⟩, distance is equal to 1.812(2) Å and comparable to ⟨Fe^{+3}–O⟩ = 1.8872(15) Å, which was observed in magnetite (Bosi et al., 2009). The tetrahedron is "flattened" because one bond distance is significantly shorter than the three others (Table 1).

In Table 2 is reported the model of the cation's distribution, using the average chemical composition determined from six different crystals. The small amount of Al (about 0.03 a.p.f.u.) is neglected for simplicity.

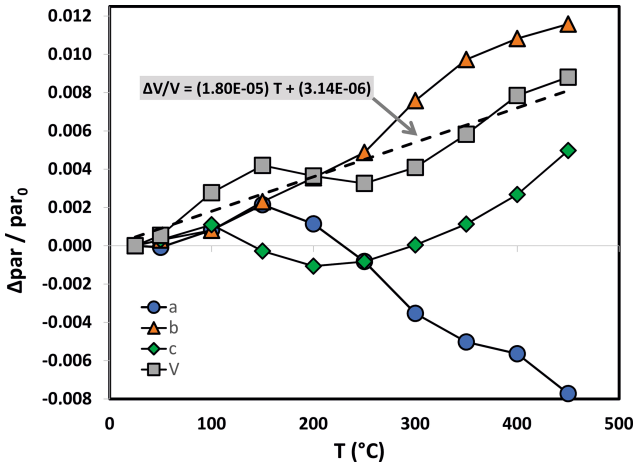

Figure 6. Unit cell normalized parameter $\Delta a/a_0$ (blue circle), $\Delta b/b_0$ (orange triangle), $\Delta c/c_0$ (green diamond) and $\Delta V/V_0$ (gray square) of paramontroseite vs. T. At $T > 350$ °C the phase is meta-stable. The linear regression of $\Delta V/V_0$ values vs. T is reported.

3.2 In situ high-temperature X-ray powder diffraction

In situ high-temperature X-ray powder diffraction data collection was carried out every 50 °C to explore the occurrence of a transformation and refine the unit cell parameters of paramontroseite. The dilatation in the 25–450 °C interval is anisotropic (Fig. 6 and Table 3): (i) a remains quasi-unchanged between 25 and 200 °C and shortens (−0.2 %) at higher temperature; (ii) b increases over the entire range investigated (1.2 %); (iii) c does not change significantly up to 200 °C and expands steadily at higher temperature (0.5 %). The thermal expansion coefficients of the unit cell parameters are not reported in the literature to our knowledge. Although the investigated range is comparatively narrow (20–450 °C) and the behavior of the unit cell parameters vs. T is irregular, we estimated the thermal expansion coefficients β using linear regression. In doing so, we found for a, b and c -2.0×10^{-5}, 3.0×10^{-5} and 0.8×10^{-5} °C^{-1}, respectively. The unit cell volume, V, shows a non-linear trend with T: it increases until 150 °C, then slightly decreases until 250 °C and finally increases beyond; the thermal expansion coefficient over the entire thermal range is 1.8×10^{-5} °C^{-1}.

At $T > 350$ °C, paramontroseite is not stable anymore and gradually decomposes into a mixture of two phases, which are identified as Fe-tetrapolyvanadate ($Fe_2V_4O_{13}$ – hereafter VFeOx) and pentoxide (V_2O_5 – shcherbinaite). In both systems, V underwent oxidation, changing from [+4] to [+5]. At the end of the transformation, VFeOx and V_2O_5 amount to ∼ 65 wt % and ∼ 35 wt %, respectively (Fig. 7).

Neglecting the small content of Al in paramontroseite and using the approximate formula unit given by $V_{0.8}Fe_{0.2}O_2$, we propose the following reaction, at $T > 350$ °C:

$$10V_{0.8}Fe_{0.2}O_2 + \frac{3}{2}O_2 \rightarrow V_4Fe_2O_{13} + 2V_2O_5.$$

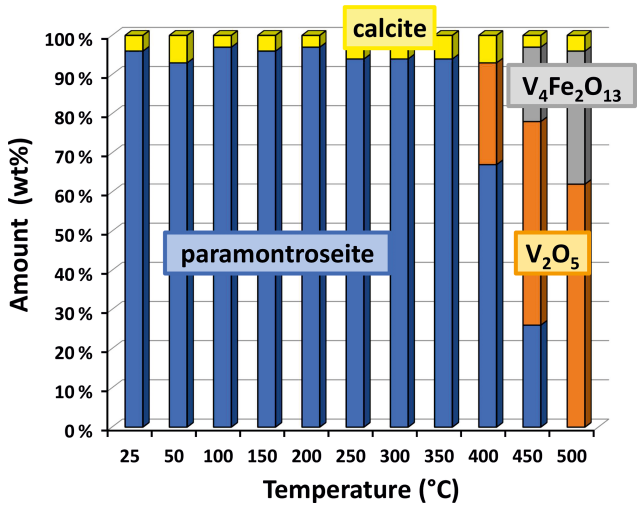

Figure 7. Phase composition (wt %) of the system under study as a function of temperature.

In V_2O_5 (orthorhombic, space group $Pmn2_1$; $a = 11.54$ Å, $b = 4.38$ Å, $c = 3.57$ Å, $V = 180.7$ Å^3; Shklover et al., 1996) each cation is bonded to five oxygen atoms, thus forming coordination polyhedra similar to irregular pentahedra. Each polyhedron shares two edges with the others (three oxygens) and one corner; the remaining oxygen atom is an unshared apex of a pentahedron. In a tetrahedral sheet, half apical oxygens point in one direction and half in the opposite direction (Fig. 8a).

In VFeOx (monoclinic, space group $P2_1/c$; $a = 8.31$ Å, $b = 9.40$ Å, $c = 14.57$ Å, $\beta = 102.23°$, $V = 1113.8$ Å^3; Permer and Laligand, 1997) the coordination polyhedra of the cations are almost inverted with respect to the paramontroseite: V forms irregular pentahedra and Fe octahedra. Couples of Fe octahedra share one edge and lie in the 001 plane; among two octahedral sheets, V pentahedra share all vertices with octahedra and/or pentahedra (Fig. 8b).

Taking the structural differences between these phases into account, we think that the high-temperature transformation occurs as a destabilization of paramontroseite and successive nucleation/growth of new phases. There is no evidence that nucleation of the new phases occurs through the formation of an intermediate amorphous phase: the refined amount of calcite (stable in the explored T interval and here used as an "internal standard") does not change with T, which allows us to exclude formation of glass.

In the iso-structural ramsdellite (MnO_2) at $T > 310$ °C, Curetti et al. (2021) observed a transformation into a rutile-type structure, at variance with paramontroseite that does not reveal such a transition. This points out that V exhibits a significantly different behavior with respect to Mn.

3.3 Raman spectroscopy on natural and heated crystals

μ-Raman measurements were performed on natural single crystals of paramontroseite, but no peak was revealed in the range 60–1050 cm^{-1}. Conversely, the crystals treated by heating for 6 h at 400 °C yielded μ-Raman patterns clearly showing peaks. The surface of the heated crystals exhibits zones of metallic black color (similar to natural paramontroseite) and brown-red "patches". Raman spectra collected from both areas gave the patterns displayed in Fig. 9. The RRUFF™ Project database reports three Raman spectra (ID R050391) measured on paramontroseite from Montrose County (Colorado) bearing a non-negligible amount of iron (8.8 wt %) like ours (∼ 20 wt %). Yet, Shvets et al. (2019) "suspect" that they actually represent the results of a crystal degradation because of the similarity to those of V_2O_5. A very good match occurs between our Raman spectra from black metallic areas (heated samples) and those available in the database, in keeping with the interpretation of Shvets et al. (2019). In the spectra recorded on the brown-red areas, new peaks appear (Table 4; red arrows in Fig. 9), at positions where just perceptible "shoulders" were visible in the pattern from the black metallic area. We think that this is reflective of the occurrence of the HT phases, i.e., V_2O_5 + VFeOx, due to V oxidation and paramontroseite decomposition.

Unfortunately, we did not find in the literature a reference Raman spectrum of Fe-tetrapolyvanadate, so we were not able to make a direct comparison; in addition, there is strong overlap of the signals with each other, making it very difficult to unfold and unambiguously assign every peak to each of the two phases that are involved.

Upon acquiring a real-time measurement on a non-treated paramontroseite for a few minutes, the crystal surface undergoes degradation under the laser beam, and, in the resulting pattern, peaks gradually emerge that match those of the database (Bernardini et al., 2020, did similar observations on ramsdellite). Therefore, we are inclined to believe that the Raman peaks reported in the database (and measured on the sample from Montrose) are ascribable to the phases that form at high T, by Fe-bearing paramontroseite decomposition (Fig. 9), as Shvets et al. (2019) suspected.

4 Conclusions

Crystal–chemical characterizations of a natural V–Fe paramontroseite have provided pieces of new information about the arrangement of the cations in the oxygen framework. In situ measurements under high-temperature conditions revealed the thermal stability range of paramontroseite and its transformation, associated with an oxidation reaction of V. In view of this, the main conclusions that could be drawn from this study are reported below.

i. V and Fe in paramontroseite do not replace one another because they occupy distinct octahedral and tetrahedral

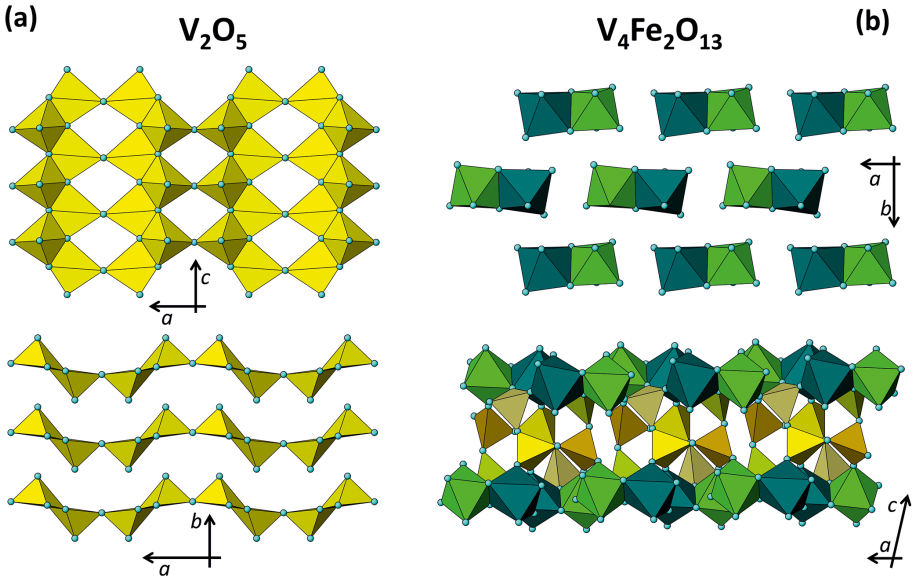

Figure 8. Structural framework of V pentahedra and Fe octahedra in V_2O_5 **(a)** and $V_4Fe_2O_{13}$ **(b)** in two different orientations.

Table 4. Refined peak positions of the Raman spectra measured on heated crystals in the brown-red and the black metallic areas. Estimated uncertainty 0.1 cm^{-1}.

Refined center position of the Raman peaks (cm^{-1})					
brown-red area	black metallic area	brown-red area	black metallic area	brown-red area	black metallic area
91.6	93.1	405.2	405.2	888.4	–
113.2	–	474.1	451.8	916.9	–
138.3	136.3	513.2	500.4	953.8	–
187.9	189.7	628.4	–	990.3	989.2
248.9	–	684.2	693.2	1009.3	–
276.0	278.2	741.3	–		
313.6	301.3	822.1	823.2		

sites, respectively. The geometrical distance between M and T positions is 1.746(2) Å, i.e., shorter than ⟨M–O⟩ [1.9954(16) Å] and ⟨T–O⟩ [1.812(2) Å], thus suggesting that it is unlikely for both sites to be occupied at the same time.

ii. Under high-T conditions, the dilatation of the paramontroseite is anisotropic: the unit cell volume shows a non-linear trend with T, characterized by three intervals, in which V increases, decreases and increases again (overall $\beta = 1.8 \times 10^{-5}\,°C^{-1}$), though a shortens, b remains almost constant until 300 °C and then increases, and c increases steadily. Paramontroseite is stable up to 350 °C. We expect that the occurrence of Fe^{3+} affects both the thermal expansion and the break-down temperature of paramontroseite, with respect to pure VO_2, though data on the latter are not available for a direct comparison.

iii. In the interval 350–400 °C, paramontroseite becomes unstable and two phases are seen to form, under V oxidation to [+5]: V_2O_5 (shcherbinaite) and $V_4Fe_2O_{13}$ (Fe-tetrapolyvanadate). Both have a structure different from paramontroseite's. In the light of this, we suggest that the V oxidation causes a complete decomposition of the parent phase with a consequent crystallization of the new ones.

iv. μ-Raman spectroscopy experiments revealed the occurrence of a transformation, as shown by the appearance of new peaks. Yet, we were not able to univocally ascribe the μ-Raman peaks, as the reference database lacks information about Fe-tetrapolyvanadate, i.e., one of the phases into which paramontroseite decomposes at high temperature.

v. There is no evidence for the formation of a rutile-type phase, at variance with what is observed for the

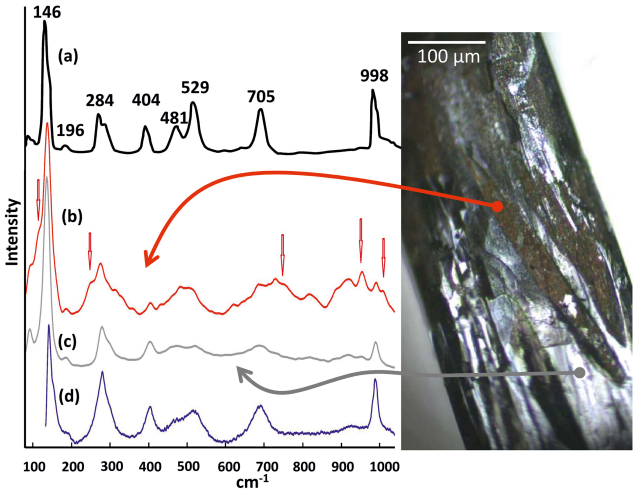

Figure 9. Comparison of Raman shift spectra measured on **(a)** pure V_2O_5 (adapted by Bhaskaram et al., 2016), **(b)** brown-red part of the heated crystal (this work), **(c)** black metallic part of the heated crystal (this work) and **(d)** natural paramontroseite from Bitter Creek Mine (RRUFF™ Project database).

iso-structural ramsdellite MnO_2, which at $T > 310\,°C$ transforms into its polymorph, i.e., pyrolusite.

Code availability. The CSD-CCDC codes 2212426–2212427 contain the CIF and FCF files (refinement results and calculated structure factors F_{hkl}). Data are available free of charge at https://www.ccdc.cam.ac.uk/structures, last access: 26 May 2023.

Data availability. Data can be obtained free of charge via https://www.ccdc.cam.ac.uk/structures (Groom et al., 2016).

Author contributions. NC and AP designed the experiment; NC carried out the experiment; NC and AP prepared the manuscript.

Competing interests. At least one of the (co-)authors is a member of the editorial board of *European Journal of Mineralogy*. The peer-review process was guided by an independent editor, and the authors also have no other competing interests to declare.

Disclaimer. Publisher's note: Copernicus Publications remains neutral with regard to jurisdictional claims in published maps and institutional affiliations.

Acknowledgements. The authors are grateful to Marco Ciriotti (President of AMI, "Associazione Micromineralogica Italiana") for advice on finding natural samples. The authors also thank Carmelo Sibio for the careful preparation of the samples. The CrisDi Interdepartmental Center and the Giovanni Scansetti Interdepartmental Centre of the University of Turin are kindly acknowledged. The authors thank Davide Bernasconi for improving the images in the manuscript.

Financial support. The present investigation was partly funded by the Italian Ministry for Education, University and Research through the MIUR Project PRIN 2017 (2017L83S77).

Review statement. This paper was edited by Giuseppe Cruciani and reviewed by two anonymous referees.

References

Bhaskaram, S., Cheruku, R., and Govindaraj, G.: Reduced graphene oxide wrapped V_2O_5 nanoparticles: green synthesis and electrical properties, J, Mater, Sci,, 27, 10855–10863, https://doi.org/10.1007/s10854-016-5194-x, 2016.

Bernardini, S., Bellatreccia, F., Della Ventura, G., Ballirano, P., and Sodo, A.: Raman spectroscopy and laser-induced degradation of groutellite and ramsdellite, two cathode materials of technological interest, RSC Adv., 10, 923–929, https://doi.org/10.1039/c9ra08662e, 2020.

Bosi, F., Hålenius, U., and Skogby, H.: Crystal chemistry of the magnetite-ulvöspinel series, Am. Mineral., 94, 181–189, https://doi.org/10.2138/am.2009.3002, 2009.

Curetti, N., Merli, M., Capella, S., Benna, P., and Pavese, A.: Low-pressure ferroelastic phase transition in rutile-type AX_2 minerals: cassiterite (SnO_2), pyrolusite (MnO_2) and sellaite (MgF_2), Phys. Chem. Miner., 46, 987–1002, https://doi.org/10.1007/s00269-019-01057-7, 2019.

Curetti, N., Bernasconi, D., Benna, P., Fiore, G., and Pavese, A.: High-temperature ramsdellite–pyrolusite transformation kinetics, Phys. Chem. Mineral., 48, 43, https://doi.org/10.1007/s00269-021-01166-2, 2021.

Evans, H. T. and Block, S.: The crystal structure of montroseite, a vanadium member of the diaspore group, Am. Mineral., 38, 1242–1250, 1953.

Evans, H. T. and Mrose, M. E.: A crystal chemical study of montroseite and paramontroseite, Am. Mineral., 40, 861–875, 1955.

Fortier, J.-P., Baloukas, B., Zabeida, O., Klemberg-Sapieha, J. E., and Martinu, L.: Thermochromic VO_2 thin films deposited by HiPIMS, Sol. Energ. Mat. Sol. C., 125, 291–296, https://doi.org/10.1016/j.solmat.2014.03.007, 2014.

Groom, C. R., Bruno, I. J., Lightfoot M. P., and Ward S. C.: The Cambridge Structural Database, Acta Cryst., B72, 171–179, https://doi.org/10.1107/S2052520616003954, 2016.

Lafuente, B., Downs, R. T., Yang, H., and Stone, N.: The power of databases: the RRUFF project, in: Highlights in Mineralogical Crystallography, edited by: Armbruster, T. and Danisi, R. M., Berlin, Germany, W. De Gruyter, 1–30, https://rruff.info/about/downloads/HMC1-30.pdf (last access: 25 May 2023), 2015.

Mingzhe, C., Qiannan, L., Zhe, H., Yanyan, Z., Guichuan, X., Yuxin, T., and Shu-Lei, C.: Designing Advanced Vanadium-Based Materials to Achieve, Adv. Energy Mater., 10, 2002244, https://doi.org/10.1002/aenm.202002244, 2020.

Ndiaye, N. M., Madito, M. J., Ngom, B. D., Masikhwa, T. M., Mirghni A. A., and Manyala, N.: High-performance asymmetric supercapacitor based on vanadium dioxide and carbonized iron-polyaniline electrodes, AIP Adv., 9, 055309, https://doi.org/10.1063/1.5091799, 2019.

Permer, L. and Laligant, Y.: Crystal structure of the tetrapolyvanadate Fe2 V4 O13, Eur. J. Sol. State. Inor., 34, 41–52, 1997.

Sejkora, J., Škácha, P., Venclík, V., and Plášil, J.: Vanad-uranová mineralizace v lomu Prachovice (Česká republika), Bull. Mineral.-Petrolog. Odd. Nár. Muz. (Praha), 21, 113–130, 2013.

Shklover, V., Haibach, T., Ried, F., Nesper, R., and Novak, P.: Crystal structure of the product of Mg^{2+} insertion into V_2O_5 single crystals, J. Sol. Stat. Chem., 123, 317–323, https://doi.org/10.1006/jssc.1996.0186, 1996.

Sheldrick, G. M.: A short history of SHELX, Acta Crystallogr. A, 64, 112–122, https://doi.org/10.1107/S0108767307043930, 2008.

Shvets, P., Dikaya, O., Maksimova, K., and Goikhman, A.: A review of Raman spectroscopy of vanadium oxides, J. Raman Spectrosc., 50, 1226–1244, https://doi.org/10.1002/jrs.5616, 2019.

Toby, R. and Von Dreele, B.: GSAS-II: The Genesis of a Modern Open-Source All-Purpose Crystallography Software Package, J. Appl. Crystallogr., 46, 544–549, https://doi.org/10.1107/S0021889813003531, 2013.

Wachs, I. E.: Catalysis science of supported vanadium oxide catalysts, Dalton T., 42, 11762–11769, https://doi.org/10.1039/C3DT50692D, 2013.

Weeks, A. D., Cisney, E., and Sherwood, A. M.: Montroseite, a new vanadium oxide from the Colorado Plateaus, Am. Mineral., 38, 1235–1241, 1953.

Wojdyr, M.: Fityk: a general-purpose peak fitting program, J. Appl. Crystallogr., 43, 1126–1128, https://doi.org/10.1107/S0021889810030499, 2010.